Linear temperature dependence of the upper critical field across the dome of the LaAlO₃-SrTiO₃ interface superconductor

L. Kuerten,[1,*] E. Fillis-Tsirakis,[1] C. Richter,[1,2] J. Mannhart,[1] and H. Boschker[1,†]

[1]*Max-Planck-Institute for Solid State Research, 70569 Stuttgart, Germany*
[2]*Center for Electronic Correlations and Magnetism, Augsburg University, 86135 Augsburg, Germany*

Numerous two-dimensional superconductors exhibit a characteristic dome-shaped dependence of the critical temperature T_c on the carrier density. The reduction of the critical temperature with increasing charge carrier density on the overdoped side of this dome is frequently related to scattering arising from conduction in multiple bands. Multiband superconductivity can be resolved by tunneling spectroscopy, but the interpretation of spectroscopic data can be ambiguous. Superconductivity in multiple bands is also expected to affect the temperature dependence of the upper critical field H_{c2} of the superconductor. We have therefore measured the temperature dependence of H_{c2} across the dome of the LaAlO₃-SrTiO₃ interface superconductor and found $H_{c2}(T)$ to be linear across the entire dome. This result places constraints on scenarios of multiband pairing in this interface superconductor.

I. INTRODUCTION

Superconducting domes are often observed in two-dimensional superconductors, such as the cuprates [1], LaAlO₃-SrTiO₃ [2,3], and in electrostatically induced superconductivity in MoS₂ [4], KTaO₃ [5], and ZrNCl [6]. Several of these superconductors are characterized by conductivity in multiple bands. In both LaAlO₃-SrTiO₃ and MoS₂, the carrier density with the highest critical temperature T_c coincides with a Lifshitz transition where an additional band becomes populated [4,7–10]. This raises the question of how the multiband nature of the electron system influences the superconducting properties. One of the fundamental properties of a superconductor that is expected to be influenced by multiband superconductivity is the temperature dependence of the upper critical field $H_{c2}(T)$. In this paper, we investigate $H_{c2}(T)$ across the superconducting dome of LaAlO₃-SrTiO₃.

At the LaAlO₃-SrTiO₃ interface [11], a two-dimensional superconducting [12] electron-liquid (2DEL) [13] exists on the SrTiO₃ side of the interface. Due to the breaking of inversion symmetry, the band structure of the 2DEL is modified with respect to the band structure of doped bulk SrTiO₃ [14]. In the LaAlO₃-SrTiO₃ system, the interface breaks the crystal symmetry and splits the degeneracy of the t_{2g} bands [15–18]. Therefore, conductivity is facilitated by a combination of bands formed from the titanium d_{xy}, d_{xz}, and d_{yz} orbitals. Depending on the growth parameters and the applied gate voltages, multiple bands can participate in conductivity at the interface [7,8,10,14,19]. Because of significant interband scattering, all bands participating in transport are expected to be superconducting. However, whether superconductivity

in LaAlO₃-SrTiO₃ is present in multiple bands has not been resolved experimentally.

In electron tunneling experiments on the LaAlO₃-SrTiO₃ interface, the superconducting gap usually appears without side peaks [3,20,21], indicating a single gap. However, because of the planar geometry of the tunneling junction, which dictates a tunneling current perpendicular to the interface, tunneling electrons can predominantly access the bands derived from the d_{xz} and d_{yz} orbitals. The d_{xy} orbital is mostly inaccessible to tunneling measurements. It is therefore a candidate to host a second band that is not visible in tunneling spectroscopy. As a reference we mention that also in early tunneling measurements on MgB₂, only a single gap was observed [22]. However, the second gap was resolved when samples with a controlled surface orientation were prepared so that both gap momenta were accessible [23].

In this paper, we use the temperature dependence of the perpendicular upper critical field H_{c2} as a probe for multiband superconductivity [24–29]. In single band s-wave superconductors, the superfluid density is almost constant at temperatures $<0.5T_c$ and the upper critical field therefore saturates at low temperature. In multiband superconductors with appreciable interband coupling, however, the superfluid density in the nondominant band increases with decreasing temperatures, because the superconducting gap in this band continues to increase with decreasing temperature [28,30]. Thus, in multiband superconductors at low temperatures, H_{c2} does not saturate; it rather continuously increases with decreasing temperature. Measurements of $H_{c2}(T)$ of the (001)-LaAlO₃-SrTiO₃ interface electron system have been performed previously in a limited temperature range and for specific carrier densities, which showed a linear behavior of $H_{c2}(T)$ [12] or minor deviations from linearity [31]. The temperature dependence of the upper critical field in (110)-oriented LaAlO₃-SrTiO₃ has also recently been investigated [32]. Furthermore, δ-doped SrTiO₃ heterostructures showed a linear $H_{c2}(T)$ [33]. In the

*lukas.kuerten@mat.ethz.ch
†h.boschker@fkf.mpg.de

Au
Ti
SrTiO$_3$
LaAlO$_3$
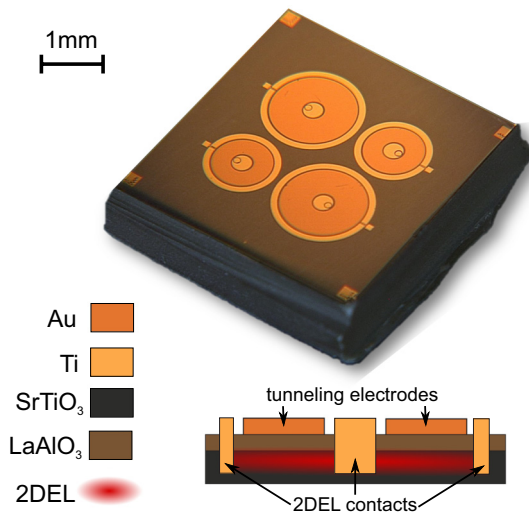2DEL

tunneling electrodes

2DEL contacts

FIG. 1. Optical micrograph showing the design of sample A in top view and schematic cross section.

present paper, we report measurements of $H_{c2}(T)$ of the (001)-LaAlO$_3$-SrTiO$_3$ interface down to lower temperatures than those probed in Refs. [12,31], at which the peculiar behavior of $H_{c2}(T)$ becomes evident. In our experiments, measurements of the tunneling current enable us to gain insight into the nature of superconductivity in all regions of the phase diagram, including the pseudogaplike [3] strongly underdoped phase in which charge transport is resistive. Our measurements show $H_{c2}(T)$ to be linear down to $0.15T_c$, consistent with the hypothesis that the LaAlO$_3$-SrTiO$_3$ interface 2DEL is a multiband superconductor.

II. EXPERIMENTAL

The data presented in this paper have been obtained on two samples. Sample A is identical in its layout to that described in Ref. [21] and was designed to allow combined tunneling and sheet resistance measurements simultaneously on the same device. For this sample, four unit cells of LaAlO$_3$ were grown by pulsed laser deposition (PLD) on a TiO$_2$-terminated SrTiO$_3$ (001) substrate at 800 °C and an O$_2$ pressure of 8×10^{-5} mbar using a laser fluence of 0.8 J cm^{-2}. Layer-by-layer growth was monitored by reflection high energy electron diffraction (RHEED), which showed clear intensity oscillations. After annealing the sample in 400 mbar O$_2$ for two hours to ensure oxygen stoichiometry, a Au capping layer was deposited by PLD onto the sample *in situ*, preventing surface degradation arising from exposure to air. The Au layer was subsequently patterned by photolithography and KI + I$_2$ etching into ring-shaped top electrodes. In the next patterning step, contacts to the 2DEL were defined by photolithography, etched with Ar$^+$ ion milling and filled *in situ* with Ti using electron beam evaporation. Four circular devices were patterned on the sample, two with a diameter of 1 mm and two with a diameter of 1.5 mm. The devices, which are shown in Fig. 1, allow both four-point sheet resistance measurements of the 2DEL between the inner and outer Ti electrodes and four-point tunneling measurements between the Au top electrode and the 2DEL. The large size of the devices ensures high

energy resolution for tunneling measurements. The outer ring electrode, when grounded during measurement, minimizes external disturbances of the electron system. By comparing the sheet resistance inside the device and between different devices, we found that the gold top electrode has only minor influence on the electron system underneath.

Sample B was fabricated using similar steps. However, the devices on this sample are of a different geometry (see Ref. [3] and supplementary therein). This geometry is well suited for probing superconductivity in tunneling measurements but limits the accuracy of sheet resistance measurements.

For electrical measurements, the devices were wire bonded to a chip carrier equipped with an Al back-gate electrode. AC measurements were performed using Stanford Research SR830 lock-in amplifiers at 8.333 Hz and preamplifiers. In order to obtain accurate temperature measurements, a RuO$_2$ sensor was fixed to the chip carrier, which gave more precise information on the sample temperature than the mixing chamber temperature sensor of the dilution refrigerator. For both samples, the carrier density was saturated by applying high positive back-gate voltages (200 V for sample A and 350 V for sample B) at low temperature before the start of measurements. This step ensures that the carrier density is independent of the gating history.

In sample A, the doping range at high back-gate voltages (V_{BG}) was not accessible because high leakage currents led to significant heating at low temperatures. Superconductivity in this sample persists over the full accessible voltage range, corresponding to carrier densities from 2×10^{13} cm^{-2} to 3×10^{13} cm^{-2}, with the critical temperature, the critical magnetic field, and the size of the gap monotonously increasing towards more negative gate voltages. At -150 V, the critical temperature (defined as the temperature at which the resistance is 50% of the normal state value) is 270 mK with a transition width of 50 mK. At this gate voltage the critical field is 0.1 T. Typical curves for a gate voltage of -100 V are shown in Figs. 2(a) and 2(b). At gate voltages of $+100$ V and 0 V, the behavior is similar.

The phase diagram of sample B has already been described elsewhere [3,8,20]. The charge-carrier density of this sample decreases with decreasing gate voltage, and macroscopic superconductivity disappears at $V_{BG} = -130$ V, with finite sheet resistance measured down to the lowest temperature. The densities of charge carriers investigated in this sample range from 8×10^{12} cm^{-2} at -200 V to 2.7×10^{13} cm^{-2} at 100 V. The optimally doped superconducting state with a T_c of 300 mK and H_{c2} of 0.2 T occurs at 0 V. Positive gate voltages are used to reach the overdoped superconducting regime.

III. RESULTS

Studying these samples, we determined the critical magnetic field as a function of back-gate voltage and temperature across their superconducting domes. On both samples, we applied magnetic fields perpendicular to the plane of the 2DEL and measured the zero-bias tunneling conductivity ($dI/dV(0V)$) from the top gate to the 2DEL. The zero-bias tunneling conductivity is a direct measurement of the magnitude of the reduction of the electronic density of states at the Fermi energy due to the superconducting gap. Thus,
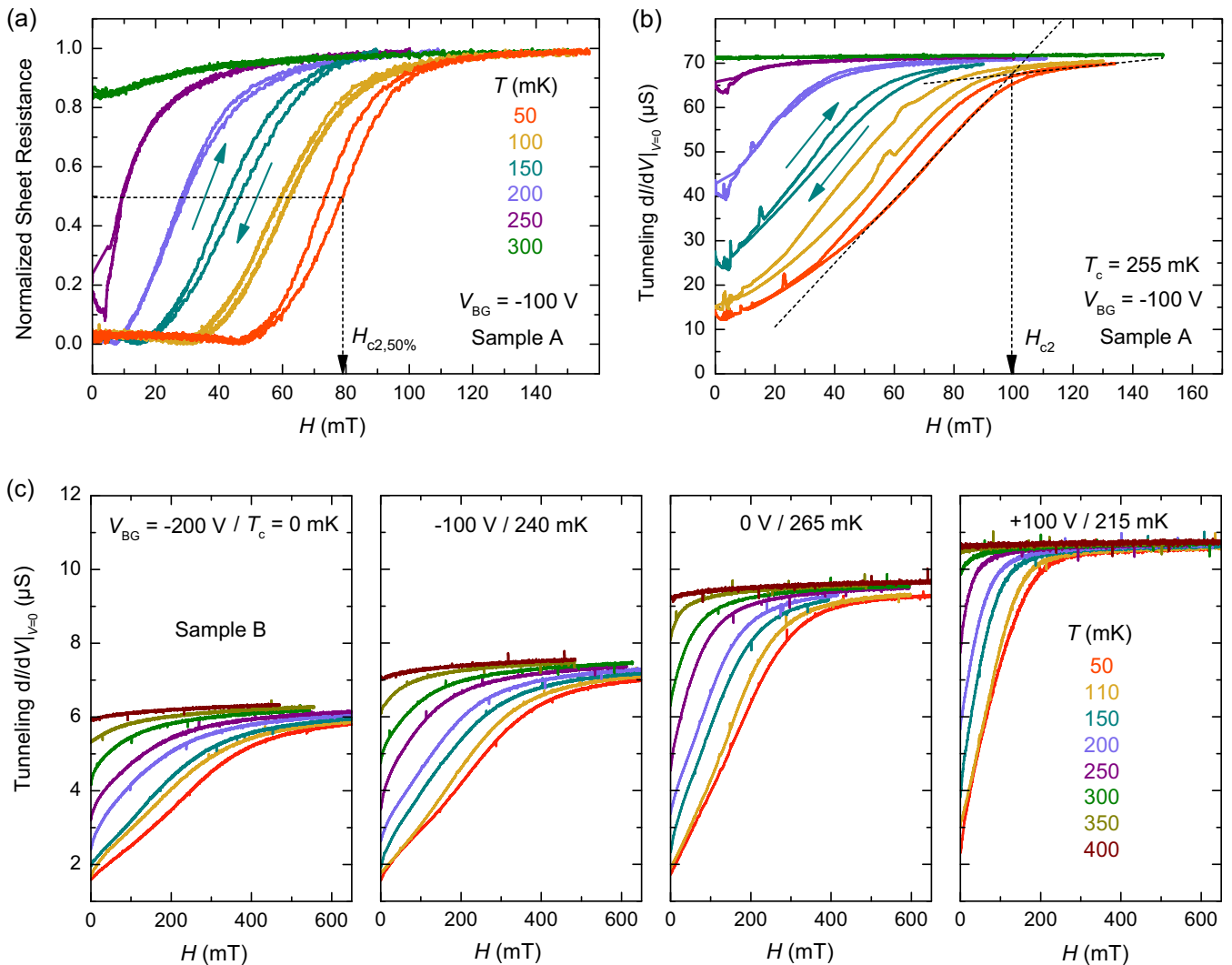
FIG. 2. $R(H)$ measurements. (a) Sheet resistance data from sample A for a back-gate voltage of -100 V. The sheet resistance is plotted as a function of applied perpendicular magnetic field for different temperatures. The difference between up and down sweeps, as indicated by arrows, is due to field-induced heating of the cryostat at very low fields and temperatures. (b) Zero-bias tunneling conductance $dI/dV(0V)$ of sample A for a back-gate voltage of -100 V plotted as a function of applied magnetic field for different temperatures. The methods employed to extract H_{c2} are illustrated for the 50 mK curves in panels (a) and (b). (c) $dI/dV(0V)$ of sample B for different temperatures at back-gate voltages of $-200, -100, 0,$ and 100 V, corresponding to the different regions of the superconducting dome. In all panels, the critical temperature T_c determined from $R(T)$ measurements at the corresponding back-gate voltage is indicated.

measuring $dI/dV(0V)$ allowed us to measure the suppression of superconductivity with magnetic field and determine H_{c2}. In addition, we measured the dependence of the sheet resistance of sample A on magnetic field at different temperatures and gate voltages.

Figure 2(a) shows the sheet resistance of sample A as a function of the applied perpendicular magnetic field at different temperatures for a back-gate voltage of -100 V. Above a well-defined field value, the resistance increases from the zero-resistance state to the normal-state resistance. The hysteresislike difference between up and down sweeps indicated by arrows is due to field-induced heating of the cryostat at very low fields and temperatures. For consistency, the following analysis only takes into account data from downward sweeps. For those sweeps, the heating effect is negligible for $H > 5$ mT. The resistive upper critical field

H_{c2} was defined as the field where the resistance has dropped to half of the normal-state value (50% criterion).

We also extracted the upper critical field from tunneling measurements using the method illustrated in Fig. 2(b). The figure shows the zero-bias tunneling conductance $dI/dV(0V)$ between the gold top electrode and the 2DEL as a function of magnetic field. At low fields, the conductivity is reduced because electrons cannot tunnel into the superconducting gap. Following the suppression of the gap with magnetic field, conductivity recovers to the normal-state value. For the tunneling conductivity, the 50% criterion cannot be applied to derive H_{c2} in a meaningful way. We therefore applied another criterion, which we refer to as "line criterion," illustrated in Fig. 2(b): Two straight lines are fitted to the curve, one in the region of maximum slope and one in the normal-conducting region. The intersection of these two lines determines the
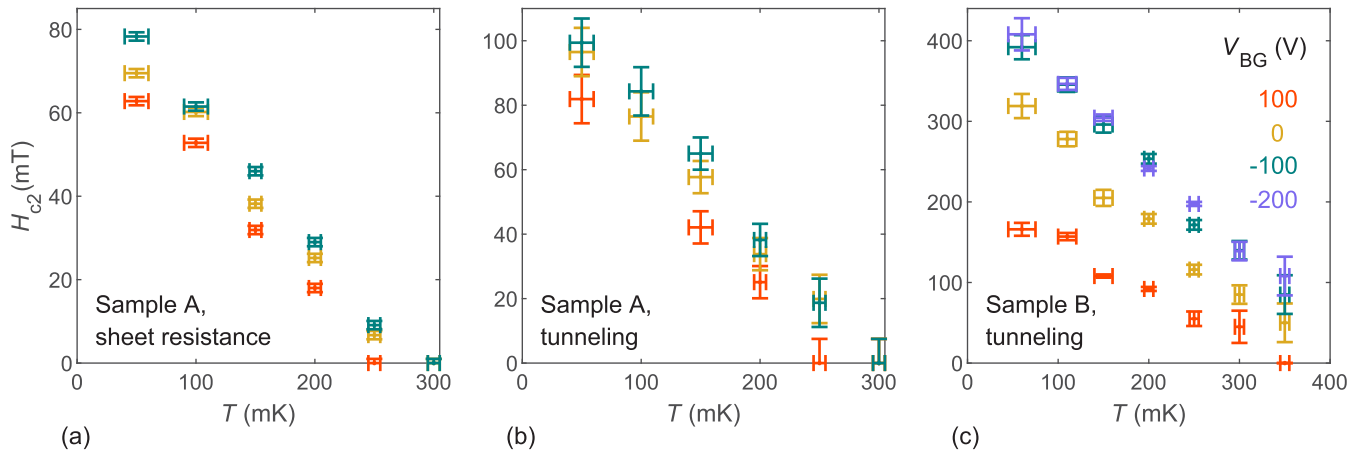
FIG. 3. The values of H_{c2} extracted from tunneling and sheet resistance measurements for both samples as a function of temperature. The vertical error bars denote the uncertainty in extracting the H_{c2} values and account for the error in locating the exact onset of the transition. Since the width of the transition in the sheet resistance is smaller, the uncertainties of the sheet resistance measurements are smaller than for the tunneling measurements. The horizontal error bars denote the accuracy of the temperature measurements affected by the H-field sweep-induced heating. This uncertainty of the temperature measurement is larger at lower temperatures where additional heating due to magnetization effects becomes significant. Comparison of panels (a) and (b) demonstrates that linear behavior is observed both in sheet resistance and tunneling measurements. Panel (c) illustrates the persistence of the linear $H_{c2}(T)$ over the entire phase diagram.

tunneling H_{c2} [20]. The width of the superconducting transition is not negligible for our measurements, as is typical for 2D superconductors. In accordance with previously published data [2,3], the suppression of the gap occurs over a broader temperature range than the resistive transition. The sheet resistance measurements therefore provide more precise results for H_{c2}. Tunneling measurements, on the other hand, can also be performed in regions of the phase diagram where transport is no longer superconducting and the temperature T_{gap} at which the superconducting gap disappears may exceed the T_c determined from transport [3]. Therefore, in the following analysis we use T_{gap} to normalize temperatures for tunneling data and T_c to normalize temperatures for transport data.

On sample A, both sheet resistance and tunneling resistance could be measured simultaneously. However, it was not possible to obtain information at all doping concentrations of the superconducting phase. On sample B, tuning the carrier concentration throughout the entire phase diagram could be achieved. Data were recorded for back-gate voltage values of $-200, -100, 0,$ and 100 V, from ≈ 60 mK to 400 mK, where the superconducting gap disappears at all gate voltages applied. Figure 2(c) shows the zero-bias tunneling conductance as a function of magnetic field for sample B at different temperatures and back-gate voltages across the superconducting dome.

From these measurements, we extracted the dependence of the critical magnetic field on temperature for samples A and B, using the criteria described above. We found that for all gate voltages and irrespective of the criterion used to extract H_{c2}, the critical magnetic field scales linearly with temperature across the entire accessible temperature range, as is shown in Figs. 3(a)–3(c). The linear behavior was found both by analyzing the in-plane transport measurements of the 2DEL [Fig. 3(a)] and by analyzing the superconducting gap of the 2DEL in the out-of-plane tunneling characteristics [Fig. 3(b)]. The linearity is also independent of the applied gate voltage. For sample B, $H_{c2}(T)$ curves at gate voltage values of $-200,$

$-100, 0,$ and 100 V are shown in Fig. 3(c), which correspond to the resistive state (where macroscopic superconductivity disappears), underdoped, optimally doped, and overdoped regions in the phase diagram of the LaAlO$_3$-SrTiO$_3$ superconductor, respectively [2,3,20]. In all cases, the $H_{c2}(T)$ curve is linear over the entire accessible temperature range, consistent with the results obtained from sample A. The critical magnetic fields extracted from sheet resistance and tunneling measurements show good quantitative agreement with each other [Figs. 3(a) and 3(b)], indicating that the electron system of the sample is homogeneous.

IV. DISCUSSION

The critical magnetic field of the LaAlO$_3$-SrTiO$_3$ 2DEL is found to vary linearly with temperature regardless of the method used to determine H_{c2}. This linearity is present for all doping concentrations: Plotting reduced H_{c2} over normalized temperature t in Fig. 4(a), we find that all data points from both samples and all back-gate voltages are described by a single straight line. This behavior deviates significantly from the prediction of a strongly curved parabolic behavior, as is expected for a standard Bardeen-Cooper-Schrieffer (BCS) superconductor [34,35]. It equally deviates from the predictions for the temperature dependence of H_{c2} calculated by Werthamer, Helfand, and Hohenberg (WHH) [36,37].

The curvature of $H_{c2}(T)$ calculated from BCS theory becomes less pronounced when corrections for a two-dimensional superconductor are taken into account as has been shown by Tinkham [38]. As we will describe below, this model gives an acceptable fit to our data.

However, because transport in LaAlO$_3$-SrTiO$_3$ occurs in multiple bands, also the scenario of multiband superconductivity is a viable candidate to explain the linearity of $H_{c2}(T)$. The characteristic dependence of the upper critical field of a multiband superconductor on temperature has been calculated
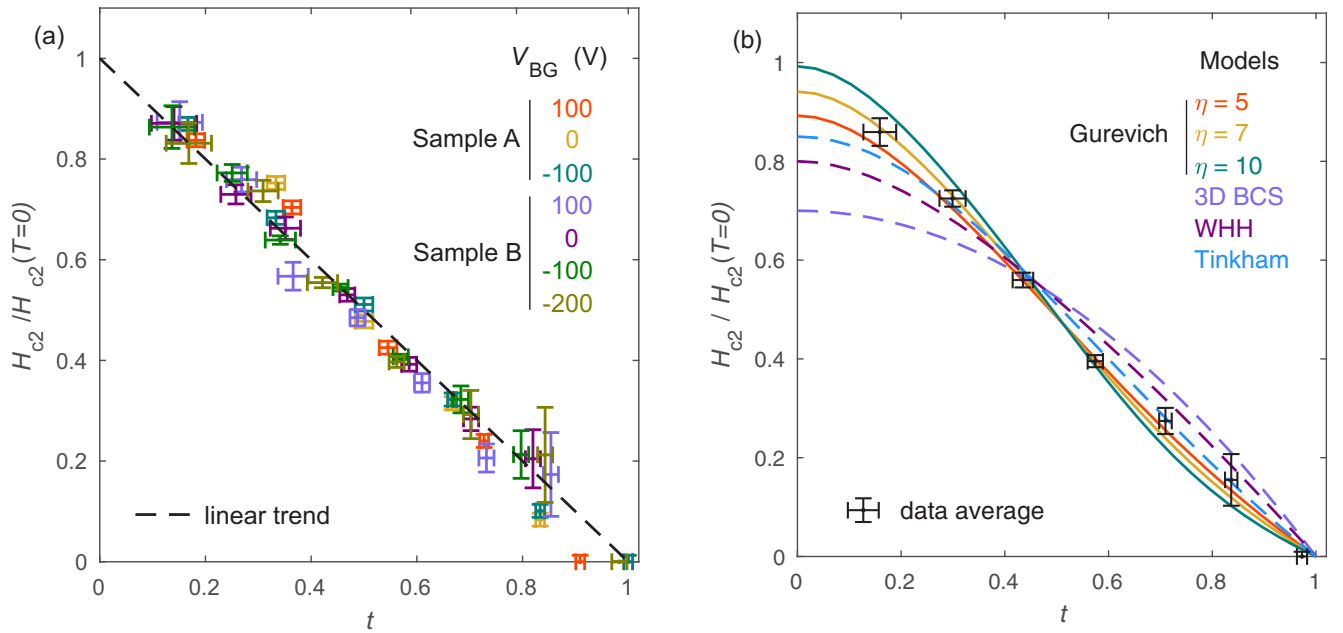
FIG. 4. (a) The combined normalized $H_{c2}(T)$ data from both samples as a function of normalized temperature t. All normalized data points are described by a single straight line. Error bars for sample A are smaller than for sample B because the 50% criterion is a more precise method of determining H_{c2} than the line criterion. (b) Averaged data compared to theoretical models. The linear behavior of $H_{c2}(T)$ clearly deviates from the standard 3D BCS curve and the WHH model. The two-dimensional corrections by Tinkham give a better fit to the data. The best fit is obtained for the Gurevich multiband model with coupling parameters for doped SrTiO$_3$ from literature [39] and a diffusivity ratio of $\eta = 7$.

by Gurevich [26]. In LaAlO$_3$-SrTiO$_3$, the scattering rate is larger than the superconducting gap, thus LaAlO$_3$-SrTiO$_3$ is a superconductor in the dirty limit. Therefore, the model of Gurevich, although conceived for MgB$_2$, is applicable also to LaAlO$_3$-SrTiO$_3$. A calculation for $H_{c2}(T)$ of the LaAlO$_3$-SrTiO$_3$ interface based on this model has been performed previously [24], but in a parameter space which is not relevant for our work. Therefore we fit our data to the model of Ref. [26], which is parametrized by the inter- and intraband coupling constants λ_{ij} and the ratio of diffusivity between the bands η. We find good agreement with the coupling parameters λ_{ij} determined by Fernandes *et al.* [39] ($\lambda_{11} = 0.14$, $\lambda_{12} = 0.02$, $\lambda_{21} = 0.008$, $\lambda_{22} = 0.13$) for a diffusivity ratio of $\eta = 7$. This set of λ_{ij} describes a system in which interband scattering is significant but not dominant. The diffusivity ratio $\eta = 7$ implies that the product of Fermi velocity and scattering time must differ significantly between the different bands. This result is consistent with the difference of Fermi velocities between different subbands observed both in *ab initio* calculations [14] and experiment [19].

The comparison between our data and the models is shown in Fig. 4(b). It is clear that the model of a three-dimensional standard BCS superconductor does not describe the data. Neither does the WHH curve calculated for the appropriate case of a dirty superconductor with dominant orbital contributions describe the observed linear behavior. Tinkham's model of a two-dimensional BCS superconductor provides an acceptable fit to the data. The best fit is obtained with Gurevich's model of multiband superconductivity with the coupling constants given above. Therefore, we conclude that if superconductivity is present in multiple bands, the system parameters must be similar to these.

Multiband superconductivity in LaAlO$_3$-SrTiO$_3$ is conceivable even though a single gap has been found in tunneling spectroscopy [3,20]. For instance, spectroscopic measurements on Nb-doped SrTiO$_3$ recently showed that this system, which is closely related to the LaAlO$_3$-SrTiO$_3$ interface, also has a single superconducting gap only, even though conductivity is present in multiple bands [40,41]. The observation of a single gap in a multiband superconductor is accounted for by Anderson's theory [42], according to which strong impurity scattering averages out the contribution of multiple bands. At the LaAlO$_3$-SrTiO$_3$ interface, a scattering rate in the same range as in bulk SrTiO$_3$ is to be expected. Therefore, the strong interband scattering is able to quench the observation of multiple gaps also in the interface superconductor.

V. SUMMARY AND CONCLUSION

In summary, comprehensive measurements of $H_{c2}(T)$ of the LaAlO$_3$-SrTiO$_3$ two-dimensional superconductor show that the dependence of H_{c2} on temperature is highly linear between $0.1T_c$ and T_c for gate voltages that cover the complete superconducting dome. These data agree best with a multiband model with diffusivity ratio $\eta = 7$ and are inconsistent with three-dimensional BCS behavior. All multiband models of superconducting systems yielding nonlinear $H_{c2}(T)$ are incompatible with our data. The observed $H_{c2}(T)$ is consistent with the single-gap behavior observed in tunneling due to strong interband scattering resulting in a single gap. These measurements raise the question why the linear $H_{c2}(T)$ is found for all gate voltages across the Lifshitz transition.

L.K. and E.F.-T. contributed equally to this work.

[1] B. Keimer, S. A. Kivelson, M. R. Norman, S. Uchida, and J. Zaanen, Nature (London) **518**, 179 (2014).

[2] A. D. Caviglia, S. Gariglio, N. Reyren, D. Jaccard, T. Schneider, M. Gabay, S. Thiel, G. Hammerl, J. Mannhart, and J.-M. Triscone, Nature (London) **456**, 624 (2008).

[3] C. Richter, H. Boschker, W. Dietsche, E. Fillis-Tsirakis, R. Jany, F. Loder, L. F. Kourkoutis, D. A. Muller, J. R. Kirtley, C. W. Schneider, and J. Mannhart, Nature (London) **502**, 528 (2013).

[4] J. T. Ye, Y. J. Zhang, R. Akashi, M. S. Bahramy, R. Arita, and Y. Iwasa, Science **338**, 1193 (2012).

[5] K. Ueno, S. Nakamura, H. Shimotani, H. T. Yuan, N. Kimura, T. Nojima, H. Aoki, Y. Iwasa, and M. Kawasaki, Nat. Nanotechnol. **6**, 408 (2011).

[6] T. Takano, Y. Kasahara, T. Oguchi, I. Hase, Y. Taguchi, and Y. Iwasa, J. Phys. Soc. Jpn. **80**, 023702 (2011).

[7] A. Joshua, S. Pecker, J. Ruhman, E. Altman, and S. Ilani, Nat. Commun. **3**, 1129 (2012).

[8] H. Boschker, C. Richter, E. Fillis-Tsirakis, C. W. Schneider, and J. Mannhart, Sci. Rep. **5**, 12309 (2015).

[9] E. Maniv, M. B. Shalom, A. Ron, M. Mograbi, A. Palevski, M. Goldstein, and Y. Dagan, Nat. Commun. **6**, 8239 (2015).

[10] A. E. M. Smink, J. C. de Boer, M. P. Stehno, A. Brinkman, W. G. van der Wiel, and H. Hilgenkamp, Phys. Rev. Lett. **118**, 106401 (2017).

[11] A. Ohtomo and H. Hwang, Nature (London) **427**, 423 (2004).

[12] N. Reyren, S. Thiel, A. D. Caviglia, L. F. Kourkoutis, G. Hammerl, C. Richter, C. W. Schneider, T. Kopp, A.-S. Ruetschi, D. Jaccard, M. Gabay, D. A. Muller, J.-M. Triscone, and J. Mannhart, Science **317**, 1196 (2007).

[13] M. Breitschaft, V. Tinkl, N. Pavlenko, S. Paetel, C. Richter, J. R. Kirtley, Y. C. Liao, G. Hammerl, V. Eyert, T. Kopp, and J. Mannhart, Phys. Rev. B **81**, 153414 (2010).

[14] Z. Zhong, A. Tóth, and K. Held, Phys. Rev. B **87**, 161102 (2013).

[15] M. Salluzzo, J. C. Cezar, N. B. Brookes, V. Bisogni, G. M. De Luca, C. Richter, S. Thiel, J. Mannhart, M. Huijben, A. Brinkman, G. Rijnders, and G. Ghiringhelli, Phys. Rev. Lett. **102**, 166804 (2009).

[16] Z. S. Popović, S. Satpathy, and R. M. Martin, Phys. Rev. Lett. **101**, 256801 (2008).

[17] Ariando, X. Wang, G. Baskaran, Z. Q. Liu, J. Huijben, J. B. Yi, A. Annadi, A. R. Barman, A. Rusydi, S. Dhar, Y. P. Feng, J. Ding, H. Hilgenkamp, and T. Venkatesan, Nat. Commun. **2**, 188 (2011).

[18] A. Rubano, M. Fiebig, D. Paparo, A. Marino, D. Maccariello, U. Scotti di Uccio, F. Miletto Granozio, L. Marrucci, C. Richter, S. Paetel, and J. Mannhart, Phys. Rev. B **83**, 155405 (2011).

[19] G. Berner, M. Sing, H. Fujiwara, A. Yasui, Y. Saitoh, A. Yamasaki, Y. Nishitani, A. Sekiyama, N. Pavlenko, T. Kopp, C. Richter, J. Mannhart, S. Suga, and R. Claessen, Phys. Rev. Lett. **110**, 247601 (2013).

[20] E. Fillis-Tsirakis, C. Richter, J. Mannhart, and H. Boschker, New J. Phys. **18**, 013046 (2016).

[21] L. Kuerten, C. Richter, N. Mohanta, T. Kopp, A. Kampf, J. Mannhart, and H. Boschker, Phys. Rev. B **96**, 014513 (2017).

[22] G. Karapetrov, M. Iavarone, W. K. Kwok, G. W. Crabtree, and D. G. Hinks, Phys. Rev. Lett. **86**, 4374 (2001).

[23] M. Iavarone, G. Karapetrov, A. E. Koshelev, W. K. Kwok, G. W. Crabtree, D. G. Hinks, W. N. Kang, E.-M. Choi, H. J. Kim, H.-J. Kim, and S. I. Lee, Phys. Rev. Lett. **89**, 187002 (2002).

[24] J. M. Edge and A. V. Balatsky, J. Supercond. Nov. Magn. **28**, 2373 (2015).

[25] G. Zhang, M. Zeleznik, J. Vanacken, P. W. May, and V. V. Moshchalkov, Phys. Rev. Lett. **110**, 077001 (2013).

[26] A. Gurevich, Phys. Rev. B **67**, 184515 (2003).

[27] D. R. Tilley, Proc. Phys. Soc. **84**, 573 (1964).

[28] V. A. Moskalenko, M. E. Palistrant, and V. M. Vakalyuk, Usp. Fiz. Nauk. **161**, 155 (1991) [Sov. Phys. Usp. **34**, 717 (1991)].

[29] Y. B. Kim, C. F. Hempstead, and A. R. Strnad, Phys. Rev. **139**, A1163 (1965).

[30] M. Tinkham, *Introduction to Superconductivity, 2nd ed.* (Dover Publications, Mineola, NY, 2004).

[31] N. Reyren, S. Gariglio, a. D. Caviglia, D. Jaccard, T. Schneider, and J.-M. Triscone, Appl. Phys. Lett. **94**, 112506 (2009).

[32] S. C. Shen, B. B. Chen, H. X. Xue, G. Cao, C. J. Li, X. X. Wang, Y. P. Hong, G. P. Guo, R. F. Dou, C. M. Xiong, L. He, and J. C. Nie, Sci. Rep. **6**, 28379 (2016).

[33] M. Kim, Y. Kozuka, C. Bell, Y. Hikita, and H. Y. Hwang, Phys. Rev. B **86**, 085121 (2012).

[34] C. J. Gorter and H. Casimir, Physica **1**, 306 (1934).

[35] B. Mühlschlegel, Z. Phys. **155**, 313 (1959).

[36] E. Helfand and N. R. Werthamer, Phys. Rev. **147**, 288 (1966).

[37] N. R. Werthamer, E. Helfand, and P. C. Hohenberg, Phys. Rev. **147**, 295 (1966).

[38] M. Tinkham, Phys. Rev. **129**, 2413 (1963).

[39] R. M. Fernandes, J. T. Haraldsen, P. Wölfle, and A. V. Balatsky, Phys. Rev. B **87**, 014510 (2013).

[40] M. Thiemann, M. H. Beutel, M. Dressel, N. R. Lee-Hone, D. M. Broun, E. Fillis-Tsirakis, H. Boschker, J. Mannhart, and M. Scheffler, Phys. Rev. Lett. **120**, 237002 (2018).

[41] A. G. Swartz, H. Inoue, T. A. Merz, Y. Hikita, S. Raghu, T. P. Devereaux, S. Johnston, and H. Y. Hwang, PNAS **115**, 1475 (2018).

[42] P. Anderson, J. Phys. Chem. Solids **11**, 26 (1959).